# ISBI 2011

# SKULL-STRIPPING WITH DEFORMABLE ORGANISMS

*Gautam Prasad*[*†], *Anand A. Joshi*[*], *Paul M. Thompson*[*], *Arthur W. Toga*[*], *David W. Shattuck*[*], *Demetri Terzopoulos*[†]

[*]Laboratory of Neuro Imaging, Department of Neurology, UCLA School of Medicine, Los Angeles, CA, USA
[†]UCLA Computer Science Department, Los Angeles, CA, USA

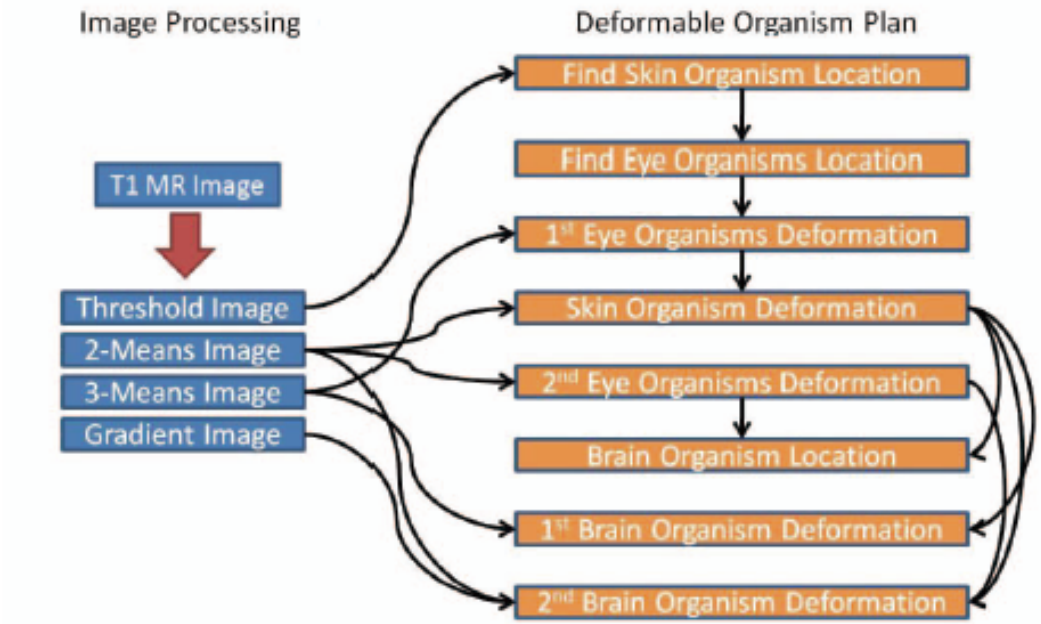


**Fig. 3.** The flow of data and steps of the algorithm. The *red* arrow shows processing steps for the image and the black arrows represent information that is being passed.

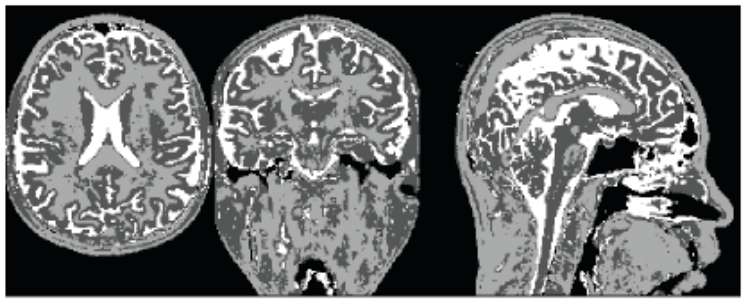

**Fig. 2.** 3-Means classification of a T1 MR image. The intensities are mapped to three different labels, segmenting it into three areas.

### 2.2.1. *Geometry and Physics*

Each deformable organism is represented geometrically as a 3D triangulated mesh. The models are initialized in the shapes of spheres that either contract or expand to find the boundary of the object being modeled. Each geometric model is deformed iteratively to model different structures in the MR images. Each vertex on the mesh is moved either inwards or outwards along the direction of the normal vector at that point. At each iteration, Laplacian smoothing is applied to the mesh to constrain the movement of each vertex in order to maintain a smooth mesh that does not pass through itself.

### 2.2.2. *Perception*

The perception layer enables the organism to sense the medical image in which it is embedded. The vertices of the triangulated mesh are represented in real coordinates embedded in a volume image represented by a set of voxels. Hence, nearest neighbor interpolation

### 2.2.3. *Motor Control*

The motor control of the organism is a function of intensities along the line normal to the mesh surface going through each vertex. The intensities along this line are from the images available to the perception layer. This layer looks for or avoids a particular intensity or relative intensity or tries to fit a certain model or statistic to the data along these lines. The intensities along the normal lines are sampled

### 2.2.4. *Behavior*

The organism has a repertoire of behaviors. Translation is a behavior that moves a particular organism rigidly without any deformation to the mesh, as does the rotation behavior. These behaviors can take into account the organism's relationship to other organisms and use information about their locations to decide how to move rigidly. Another behavior is the local deformation of the mesh. This behavior

### 2.2.5. *Cognition*

The cognitive layer is created by putting together a set of behaviors to accomplish certain goals. Different behaviors can be activated dynamically depending on what goals have been accomplished or what features have or need to be located.

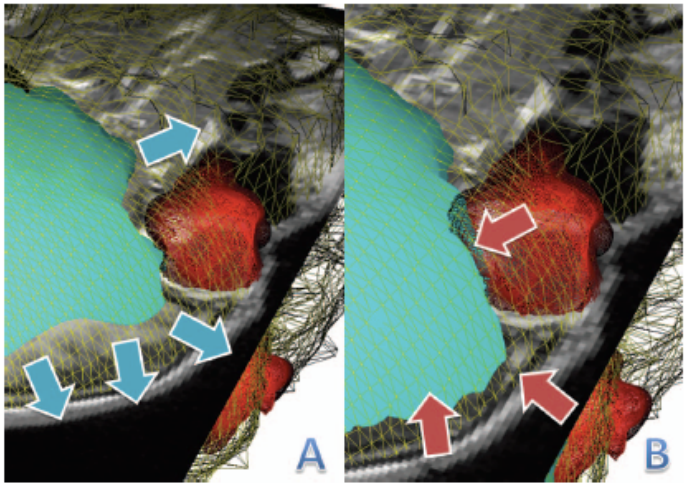


**Fig. 5.** Interactions between the brain (*cyan*), eye (*red*), and skin (*yellow*) organisms. The arrows (*blue*) in Subfigure A show how the brain organism is expanding and Subfigure B has arrows (*red*) showing how its movement is restricted by the other organisms.

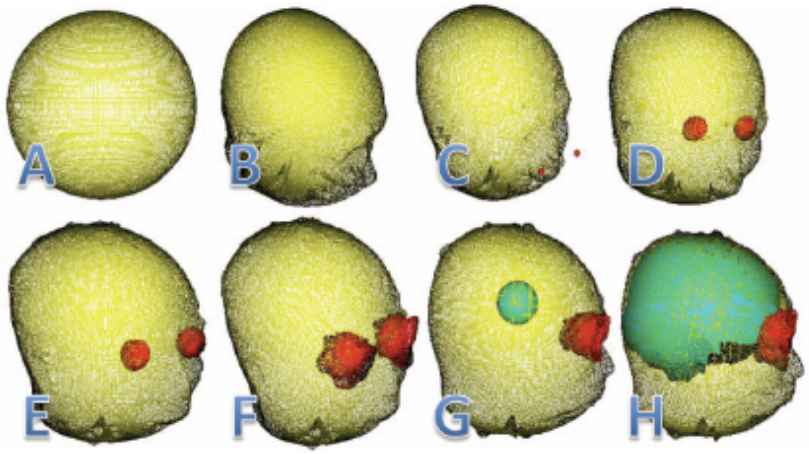


**Fig. 4.** This figure shows the sequential steps that the skin (*yellow*), eye (*red*), and brain (*cyan*) organisms use to skull-strip the head im-

| Method | Jaccard | Dice | Sensitivity | Specificity |
|---|---|---|---|---|
| DO | 0.8954±0.0288 | 0.9446±0.0163 | 0.9616±0.0129 | 0.9864±0.0082 |
| BSE | 0.9431±0.0282 | 0.9705±0.0158 | 0.9747±0.0334 | 0.9941±0.0019 |
| BET | 0.9310±0.0089 | 0.9642±0.0048 | 0.9875±0.0117 | 0.9892±0.0014 |
| HWA | 0.8537±0.0184 | 0.9210±0.0107 | 0.9992±0.0003 | 0.9695±0.0053 |

interactions during the skull-stripping process. The skin organism is initialized as a large spherical triangulated mesh that is deformed into the surface of the head using the threshold of the initial MR image (Fig. 4A and 4B). The skin organism is then processed to locate the nose. This information is used to locate the eyes (Fig. 4C and 4D). Figure 4D shows the two eye organisms expanded to the full size of the eye by sensing the 3-Means classification of the MR image. Once this is complete, the skin organism again deforms to locate the area surrounding the brain by deforming through the eyes by sensing their locations and by using edge information from the 2-Means classified image as shown in Fig. 4E. In Fig. 4F, the eyes are again deformed by sensing the 2-Means image to take into account the surrounding tissues and to restrict more areas that the brain organism may try to expand into. Then using the location of the eyes and skin meshes a brain organism is spawned (Fig. 4G) that deforms itself to match the classification of tissues in the 3-Means image and to stay within the skin mesh and complete the segmentation of the brain (Fig. 4H).

# A NEW CLASSIFIER FEATURE SPACE FOR AN IMPROVED MULTIPLE SCLEROSIS LESION SEGMENTATION

*X. Tomas-Fernandez, Simon K. Warfield*

Computational Radiology Laboratory, Department of Radiology, Children's Hospital Boston.

## 2. METHODS

### 2.1. Overview

We propose a novel approach to local MS lesion characterization for segmenting brain MRI of MS patients. Our goal is to take aligned T1w, T2w, and FLAIR MR images of an MS patient, detect voxels with an abnormal intensity level when compared to the expected value in a population of healthy subjects.

Our algorithm starts with a library of MRI images representing typical healthy subjects comparable in age to the study subject. Each reference subject image is then registered to the MS patient being segmented. Because MR image intensity varies from scan to scan due to the MRI acquisition process, intensity levels from each reference subject were normalized to match the intensity distribution in the MS patient. Finally, intensity levels between the study subject and the reference population were compared, voxel-by-voxel, by means of the Mahalanobis distance.

The local comparison between the study subject and a reference population of intensity values yields a measurement of the MS subject voxel intensity typicality that highlights brain locations with an unexpected intensity value such as MS lesions.

### 2.2 Reference Healthy Population Data

To evaluate the typicality of voxel intensity value from an MS subject, a group of 15 volunteers was used as the normal reference database.

After image acquisition, the T2w and FLAIR images were aligned to the T1w scan. In addition, all acquired MR images were re-oriented to an axial orientation and then the intra-cranial cavity was manually segmented.

### 2.3 Healthy Population Non-Rigid Registration

To evaluate a voxel's intensity value typicality, both the study subject and the reference database have to be aligned to the same reference space. Due to anatomical variability among subjects and the presence of MS lesions, a robust, block-matching based non-linear registration was used; this method extended the rigid registration algorithm proposed by [5].

### 2.4 Intensity Normalization

Because of the anatomical abnormalities (MS lesions) present in the scans we want to normalize, an algorithm that does not rely on any pre specified model was chosen. To this purpose, we used the intensity normalization method proposed in [6]. Weisenfeld et al. developed a novel approach for normalizing the intensities within an image to best match a supplied histogram model, which can be generated by any representative subject, allowing to proceed without assumptions about the shape of the histogram or the specific contribution of a given class of tissue.

For our purposes, a histogram model was provided to the intensity normalization algorithm for each of the MR modalities (T1w, T2w and FLAIR) from the MS patient. Finally, intensity levels from each reference subject were normalized to match the given histogram model.

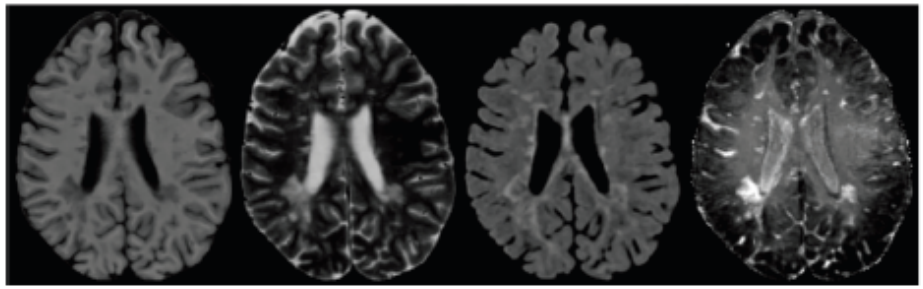

Figure 1: *Demonstration of the proposed extended feature space. From left to right: T1w scan, T2w scan, FLAIR scan, and Mahalanobis distance map. Notice how higher values in the Mahalanobis distance map correspond with MS lesions (hyper- or hypo-intensity voxels in anatomical MRI).*

### 2.5 Classifier Extended Feature Space Generation

Mahalanobis distance is a measure between two data points in the space defined by relevant features. Since it accounts for unequal variances as well as correlations between features; it will adequately evaluate the distance by assigning different weights or importance factors to the features of data points. This weighting will assign components with high variability *less* weight than components with low variability. The Mahalanobis distance is written as:

$$M\left(x_i\right)=\sqrt{\left(x_i-\mu_i\right)^T \Sigma_i^{-1}\left(x_i-\mu_i\right)}$$

Equation 1*: Mahalanobis distance*

where $x_i$ is a vector composed by the MS subject, T1w, T2w, and FLAIR scans intensity values at voxel *i*, $\mu_i$ is the mean intensity vector at the healthy reference population, and $\Sigma_i$ is the healthy population intensity covariance matrix at the location of voxel *i*. An image based on this equation is depicted in Figure 1.

## 3. VALIDATION

To evaluate the performance of this novel extended feature space, training subjects from the MS MICCAI 2008 database were used. The training database consists of 20 subjects provided by the University of North Carolina at

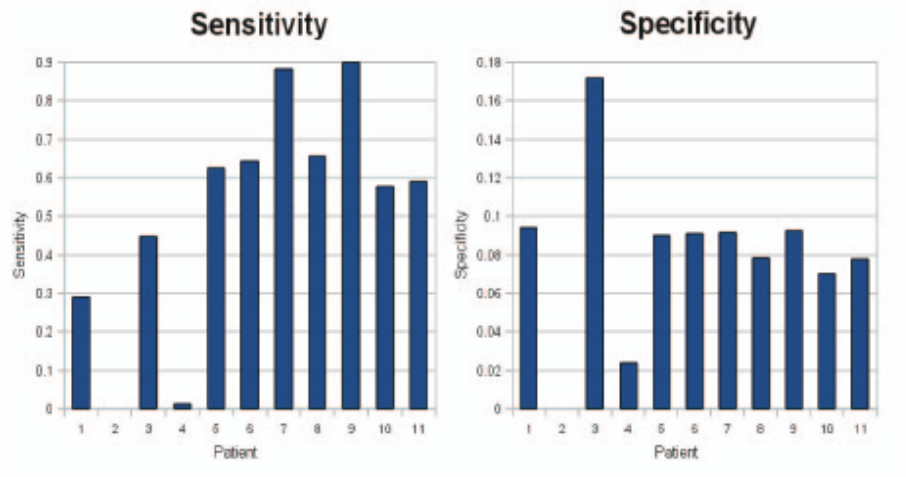


Figure 2: *Intensity outliers MS lesion classification sensitivity and specificity values.*

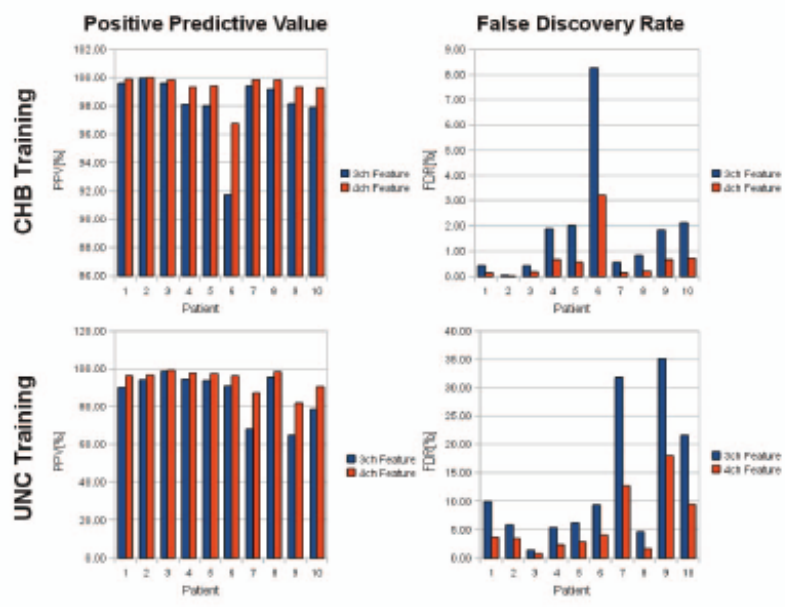


Figure 4: *MS lesion PPV and FDR values. Reported in blue are intensity feature space results; in orange, the extended feature space results. The extended feature space allows a much more precise MS lesion segmentation.*

# SURFACE-BASED METHOD TO EVALUATE GLOBAL BRAIN SHAPE ASYMMETRIES IN HUMAN AND CHIMPANZEE BRAINS

*Marc Fournier[1], Benoît Combès[1], Neil Roberts[2], Simon Keller[3], Tim J. Crow[4], William D. Hopkins[5,6] and Sylvain Prima[1]*

[1]INSERM, IRISA-INRIA VisAGeS Project-Team, F-35042 Rennes, France
[2]CRIC, Queen's Medical Research Institute, Edinburgh, U.K.
[3]Department of Neurology, University of Münster, 48149 Münster, Germany
[4]SANE POWIC, Warneford Hospital, University of Oxford, UK
[5]Department of Psychology, Agnes Scott College, Decatur, Georgia
[6]Division of Psychobiology, Yerkes National Primate Research Center, Atlanta, Georgia

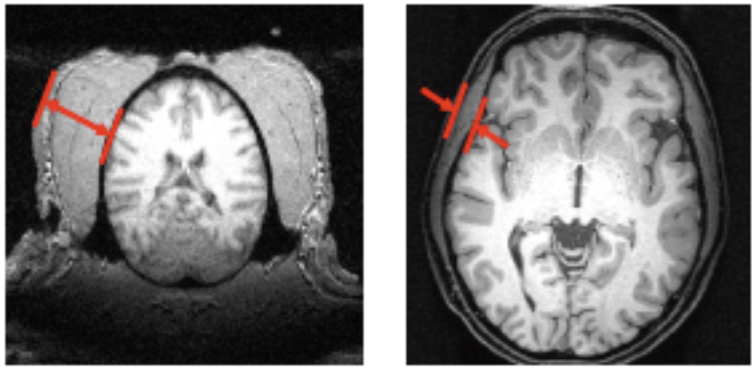

(a) Chimpanzee axial (b) Human axial

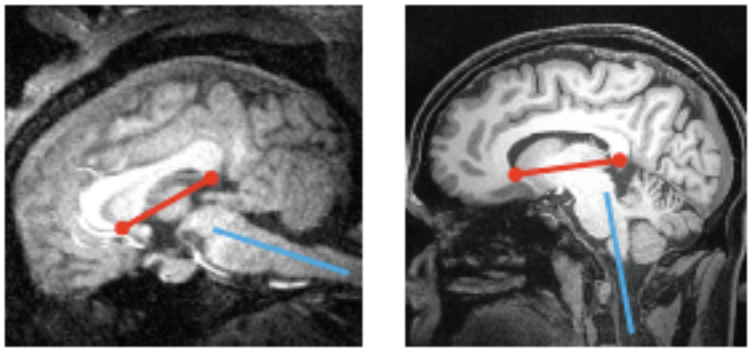

(c) Chimpanzee sagittal (d) Human sagittal

**Fig. 1. Human and chimpanzee brain differences.** (a) and (b) axial views show the surrounding tissues of the brain are thicker in chimpanzee. (c) and (d) sagittal views show different relative orientations of the anterior-posterior commissures and the spinal cord. (a) and (b) show on the same scale that the chimpanzee brain size is smaller than the human one.

## 2.2. Brain global shape computation

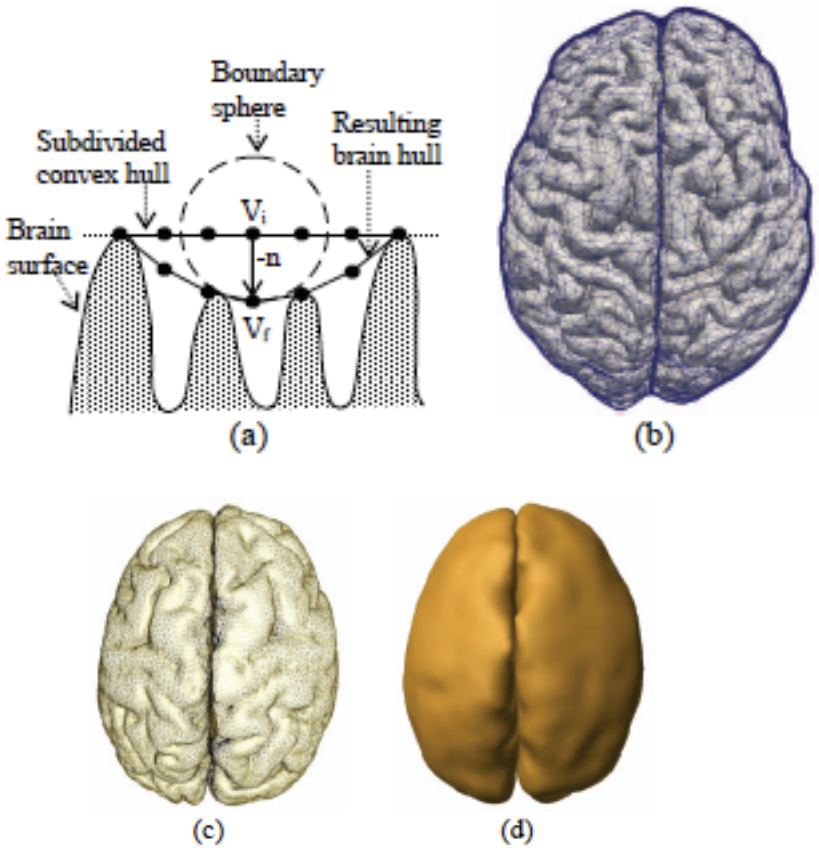


**Fig. 2. Brain hull mesh processing illustration.** (a) Brain hull algorithm computation with: $V_i$ the initial vertex position of the subdivided convex hull; $V_f$ the final vertex position of the brain hull; -n the opposite normal vertex displacement direction. (b) Brain hull meshes superposed on a human brain hemispheric surfaces. (c) A chimpanzee brain hemispheric meshes output from BrainVisa. (d) The chimpanzee hemispheric brain hulls computed.

## 2.3. Brain bilateral asymmetries evaluation

The typical *Yakovlevian torque* human brain asymmetry of right-handed subjects is illustrated in Figure 3 as a

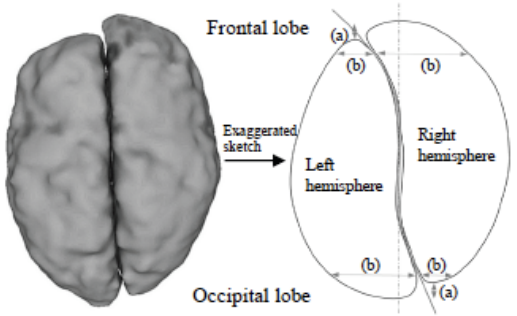


**Fig. 3. Global brain asymmetries in right-handed human subjects when viewed from above.** (a) Anterior (resp. posterior) protrusion of the brain in the right as compared to the left frontal lobe (resp. in the left as compared to the right occipital lobe). (b) Leftward frontal lobe and rightward occipital lobe deviation of the inter-hemispheric fissure.

• *First step: Finding the symmetry plane.*
We define the approximate symmetry plane $P$ of a mesh $X$ as the one best superposing $X$ and its reflection $S_P(X)$ about $P$. For that, we consider $X$ as a noised version of $S_P(X)$. This allows to consider each point $xi$ of $X$ as the realization of a random variable whose distribution is a mixture model composed of card($X$) Gaussian laws $N(S_P(x_k), \sigma^2 I)$, $x_k \in X$. Then we define the optimal reflection $S_P$ as a ML estimate, which is computed using an EM algorithm. The use of a multiscale strategy and of a truncated Gaussian kernel allows a fast, accurate and robust estimation of the plane [20].

• *Second step: Registering $X$ on $S_P(X)$.*

Once P is known, we define the asymmetry field of $X$ as $(t(x) = T(x) - x)_{x \in X}$ where $T$ is the non linear transformation best superposing $X$ and $S_P(X)$. For that, we consider $T(S_P(X))$ as a noised version of $X$ (here $S_P$ is known). Then we design a MAP approach by specifying i) a prior on $T$ (a global affine model + a local order-one Tikhonov regularization on the linear component (t(x))_x), ii) a mixture density for the set $T(S_P(X))$ and iii) a priori probabilities of matching between points of the two meshes (using geometrical descriptors almost invariant to the unknown transformation). Then, this MAP problem is solved using an EM algorithm [21].

*2.3.2 Generation of a mean shape & projection of the mapping*

• *First step: Computing the mean shape*

Individual asymmetry maps $S^X$ $(X \in \{X_1,...,X_n\})$ have to be put in a common geometry to be compared. For this purpose, we compute the mean mesh $M$, defined as the mesh closest to all the meshes in the dataset (in a sense to be defined). In practice, we formulate the mean shape estimation as an iterative scheme that consists in the successive estimation of i) the mean shape and ii) the optimal similarity transformations between each mesh and the mean mesh [22].

• *Third step: Mapping the asymmetry field*

In order to provide specific results, we choose to analyze the asymmetry field by looking at its three components separately. This simply consists in projecting the asymmetry vector on the three coordinate axes and this yields the:

- postero-anterior component (difference in protrusion);
- left-right component (difference in width);
- head-foot component.

In the following, we call $s_i^X$ the scalar asymmetry mapping at point $x_i$ of mesh $X$ and $S^X$ the asymmetry map of $X$. Each subject has thus three asymmetry maps.

• *Second step: Individual projection of the asymmetry mapping*

Together with the mean shape $M$, the previous algorithm provides us with the a posteriori probability that each point $m_i$ of $M$ is matched with a point $x_j$ of $X$; we call this probability $A_{ij}$ ($\sum_j A_{ij} = 1$). This probability is used to project each individual asymmetry map on $M$. We call $s_i^{X \to M}$ the mapping information of $X$ projected on point $m_i$ of $M$ and define it as $s_i^{X \to M} = \sum_j A_{ij} s_i^X$.

• *Third step: Population statistical asymmetry maps*

At this point we now have a collection of $n$ (×3) scalar asymmetry maps $S^{X_1 \to M}, \ldots, S^{X_n \to M}$ projected on a common mean mesh $M$. We compute a point-wise mean and t-test (corrected for multiple comparisons) on each of the three components of the asymmetry field over the population. The correction for multiple comparisons is performed as described in [23] by i) fixing a supra-threshold $p = 0.05$, ii)

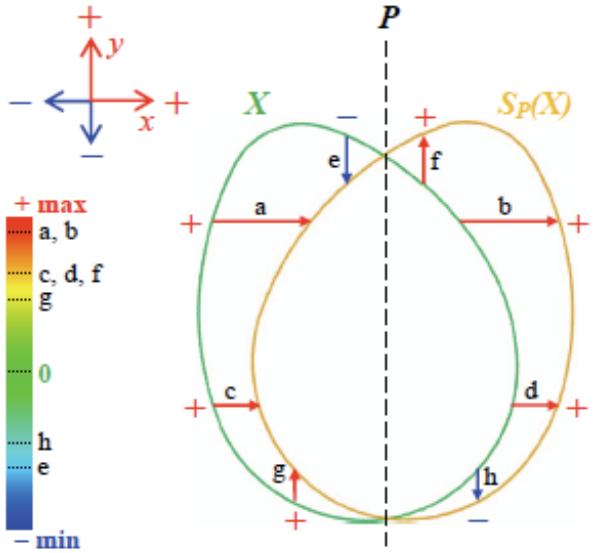


**Fig. 4. Asymmetry maps direction definition.** Orthogonal components of the deformation field which are in the same (resp. opposite) direction as their positive axis definition have positive (resp. negative) values. A color map is used to represent the signed scalar values of the deformation field.

significant. The p-values maps are computed according to the t-test with the null hypothesis that there is no asymmetry at the significance level p=0.05 (corrected). Red color indicates with more confidence regions with asymmetries.

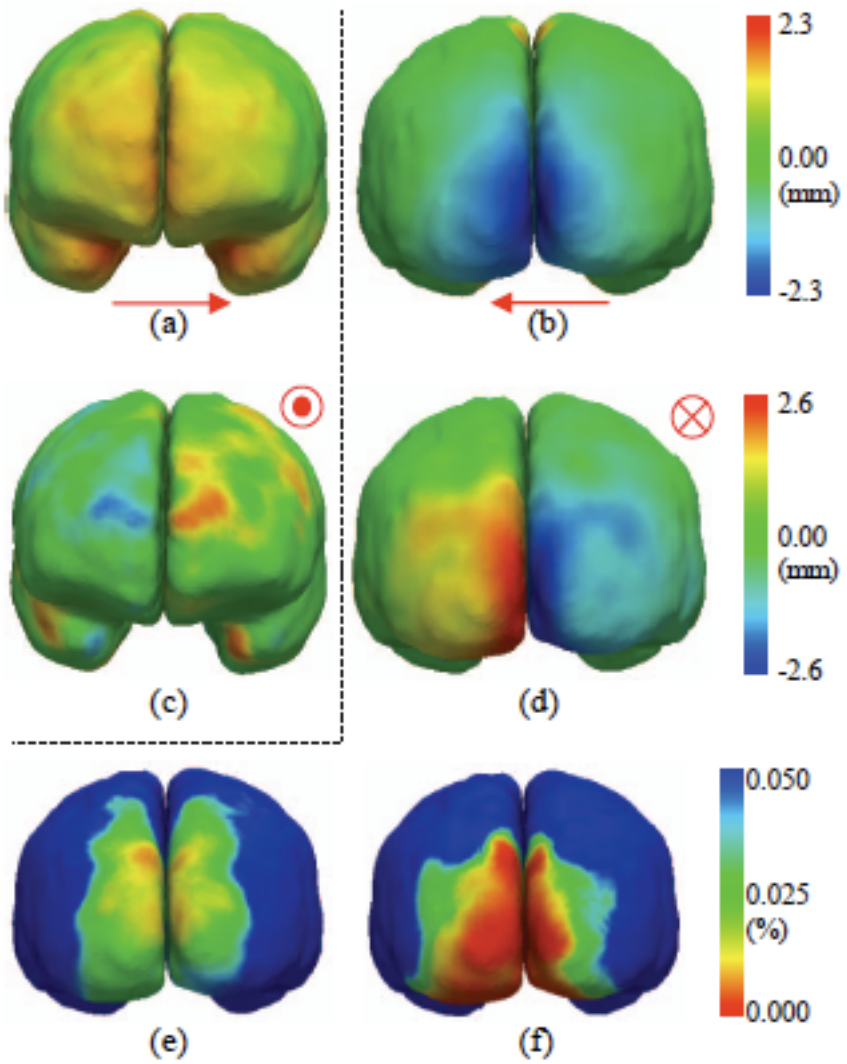


**Fig. 6. Humans asymmetry maps and p-values.** (a) Front view of right-left component. (b) Back view of right-left component. (c) Front view of posterior-anterior component. (d) Back view of posterior-anterior component. (e) p-values back view of right-left component (resp. to b). (f) p-values back view of posterior-anterior component (resp. to d).

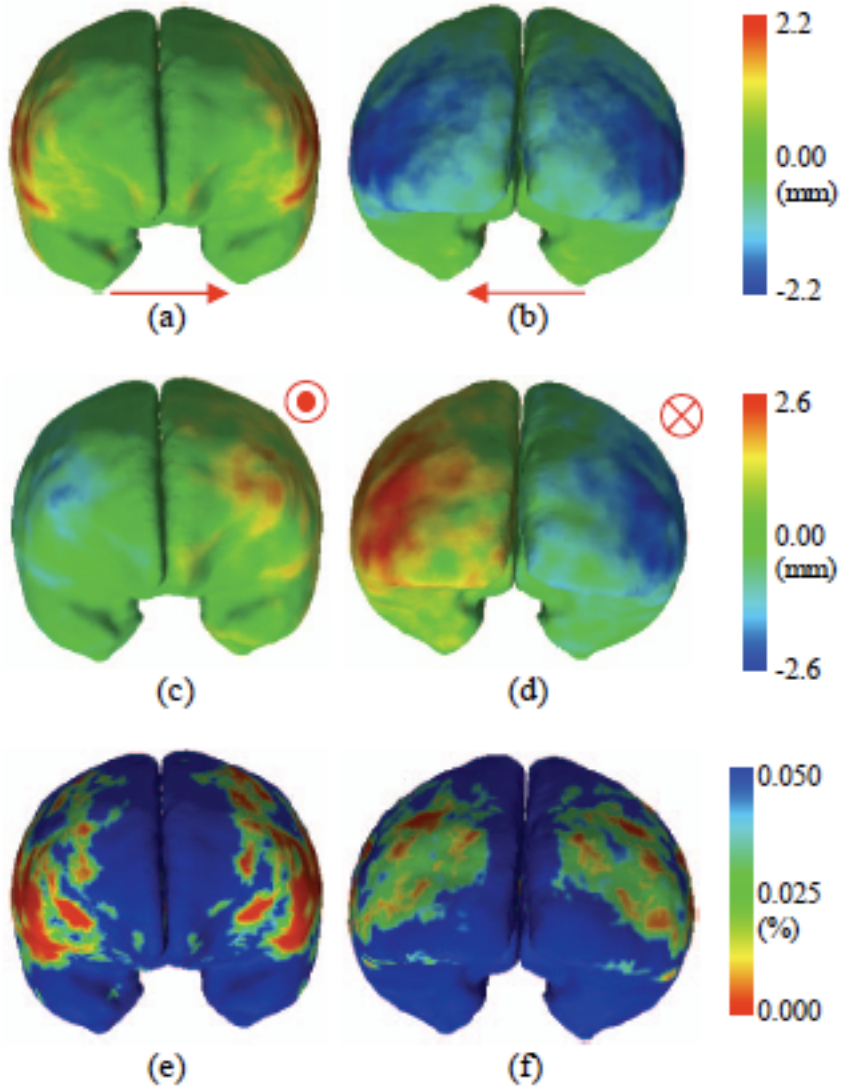


**Fig. 7. Chimpanzees asymmetry maps and p-values.**
(a) Front view of right-left component. (b) Back view of right-left component. (c) Front view of posterior-anterior component. (d) Back view of posterior-anterior component. (e) p-values front view of right-left component (resp. to a). (f) p-values back view of right-left component (resp. to b).

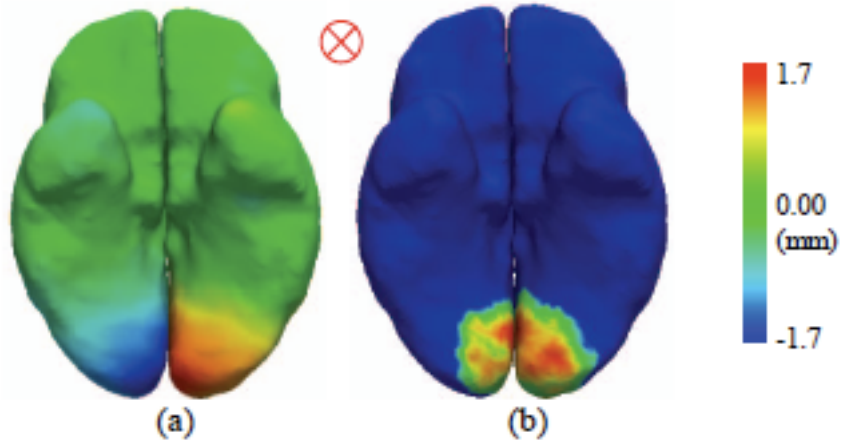


**Fig. 8. Humans foot-head deformation field component.**
(a) Bottom view of asymmetry map. (b) Bottom view of p-values. The color bar legend is for the asymmetry map. P-values have the same legend as previous figures (0; 0.05).

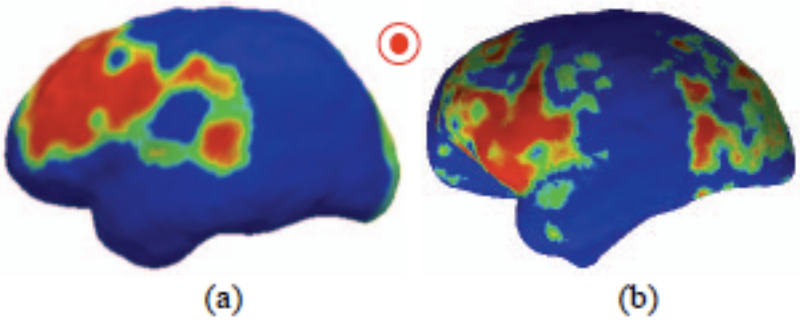


**Fig. 9. Chimpanzees and humans right-left p-values.**
(a) Humans left side view. (b) Chimpanzees left side view. P-values have the same legend as previous figures (0; 0.05) for both populations.